Three-dimensional receiver deghosting of seismic streamer data using L1 inversion and redundant extended radon dictionary

Sun, Yimin; Verschuur, Eric

DOI
10.1111/1365-2478.12615

Publication date
2018

Document Version
Final published version

Published in
Geophysical Prospecting

Geophysical Prospecting

EAGE EUROPEAN ASSOCIATION OF GEOSCIENTISTS & ENGINEERS

Geophysical Prospecting, 2018, **66**, 987–1003 doi: 10.1111/1365-2478.12615

Three-dimensional receiver deghosting of seismic streamer data using L1 inversion and redundant extended radon dictionary

Yimin Sun[1]* and Eric Verschuur[2]

[1]*EXPEC ARC GRC Delft, Aramco Overseas Company B.V., 2628 ZD Delft, The Netherlands, and* [2]*Delft University of Technology, 2600 GA Delft, The Netherlands*

Received February 2017, revision accepted November 2017

ABSTRACT

In this paper, we propose a novel three-dimensional receiver deghosting algorithm that is capable of deghosting both horizontal and slanted streamer data in a theoretically consistent manner. Our algorithm honours wave propagation phenomena in a true three-dimensional sense and frames the three-dimensional receiver deghosting problem as a Lasso problem. The ultimate goal is to minimise the mismatch between the actual measurements and the simulated wavefield with an L1 constraint applied in the extended Radon space to handle the underdetermined nature of this problem. We successfully demonstrate our algorithm on a modified three-dimensional EAGE/SEG Overthrust model and a Red Sea marine dataset.

Key words: Data processing, Deghosting, Inversion.

INTRODUCTION

Receiver deghosting of seismic streamer data is a longstanding challenge. The air–water interface is a strong reflector; hence, acoustic waves are reflected downward at the interface and interfere with the upgoing wavefield at the streamer locations. This is the well-known receiver ghost effect in marine streamer seismic data acquisition, which causes a notch in the trace frequency spectrum and can result in distortions of both phase and amplitude. Receiver deghosting strives to remove the receiver ghost reflection from marine seismic streamer data. With the advancement of marine broadband data acquisition and processing, it is more crucial than ever to apply proper 3D receiver deghosting technologies to better preserve both bandwidth and resolution in recorded data.

Many receiver deghosting techniques have been proposed. Weglein *et al.* (2002), Ramirez and Weglein (2009), Amundsen and Zhou (2013), and Amundsen, Weglein and Reitan (2013a) use Green's theorem as the general theoretical framework in deghosting. Fokkema and van den Berg (1993) and Riyanti *et al.* (2008) resorted to a mixed-domain inversion. Posthumus (1993) and Ferber, Caprioli and West (2013) used streamers at different depths to deghost. Soubaras (1996); Carlson *et al.* (2007); Robertsson *et al.* (2008); Ozbek *et al.* (2010); Kamil and Caprioli (2014); Kamil, Yadari and Vassallo (2014); and Poole (2014) proposed to use multicomponent data for receiver deghosting. Wu *et al.* (2014) and Wang, Ray and Nimsaila (2014) used a progressive sparse $\tau - p_x$-p_y inversion method to perform 3D joint deghosting and crossline interpolation using single-component pressure data. Kragh *et al.* (2004) and Amundsen *et al.* (2005) proposed to use the approximated pressure gradient to remove the ghost signals. Roberts and Goulty (1990), Soubaras (2010), and Amundsen *et al.* (2013b) applied deconvolution to suppress the ghost signals. Wang and Peng (2012) proposed a bootstrap approach, which first builds the mirror data using ray tracing and then compares the recorded data with the mirror data to estimate the deghosting operator. Berkhout and Blacquiere (2014) pointed out the similarity between deghosting and seismic deblending and therefore proposed to handle deghosting just like deblending. Egan, El-Kasseh and Moldoveanu (2007) demonstrated deghosting with over/under source acquisition. Rickett (2014) used joint interpolation deghosting to achieve genuinely 3D deghosting. Beasley, Coates and

*E-mail: sun.delft@gmail.com

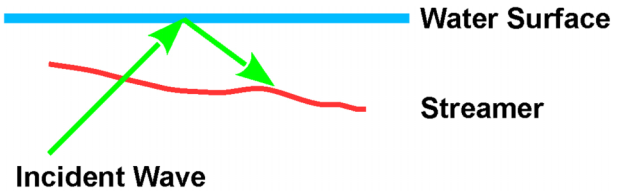

Figure 1 Schematic of streamer data acquisition. Streamers could be in any shape in reality: curved, horizontal, slanted, etc.

Ji (2013a); Beasley *et al.* (2013b); and Beasley and Coates (2014) proposed a wave equation deghosting method, which strives to honour wave propagation and causality as much as possible.

For 3D receiver deghosting, almost all the reported methods require dense wavefield sampling, but in real data acquisition, the crossline interval is normally much larger than the inline interval (typically, the ratio of inline interval to crossline interval varies between 1:4 and 1:16), which violates this fundamental assumption. As a trade-off, most methods choose either to work only on dense 2D inline data (Beasley *et al.* 2013a, 2013b; Beasley and Coates 2014; Berkhout and Blacquiere 2014) or make a 1D propagation assumption (Soubaras 1996). Rickett (2014) utilised interpolation in his method explicitly as an independent operation; however, interpolation for real data is not trivial, which makes it difficult to optimally apply both steps without a propagation of errors. As a result, for 3D field data, the receiver deghosting challenge is actually two-phase, which involves handling wavefield undersampling issue, followed by the actual receiver ghost signal removal.

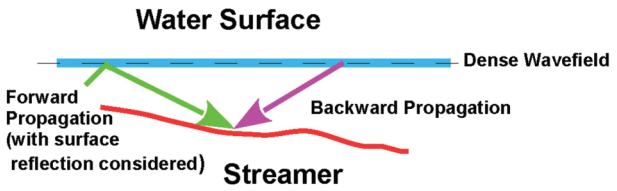

Figure 2 Schematic of our proposed solution.

In this paper, we propose a novel 3D receiver deghosting algorithm that is capable of dealing with both horizontal and slanted streamers in a theoretically consistent manner. Our method honours 3D wave propagation phenomena and simultaneously reconstructs the deghosted wavefield in a self-consistent manner. In addition, we also propose a redundant extended Radon dictionary to be used in our inversion. Our algorithm frames the 3D receiver deghosting problem as a Lasso problem (Tibshirani 1996), and the ultimate goal is to minimise the mismatch between the actual measurements and the simulated wavefield, with an L1 constraint in our extended Radon space to handle the underdetermined nature of this problem. We demonstrate our algorithm on data generated from a realistic modified 3D EAGE/SEG Overthrust model and a Red Sea marine dataset.

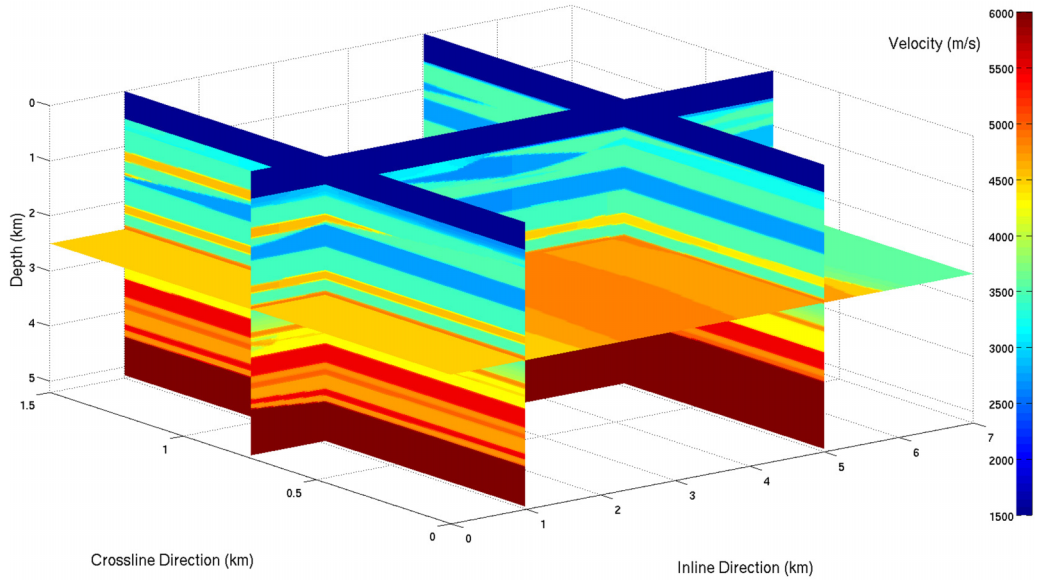

Figure 3 The modified 3D EAGE/SEG Overthrust model with a 500 m-thick water layer on top. The corresponding density model is built using Gardner's equation, except for the water layer where the density is set to 1000 kg/m^3.

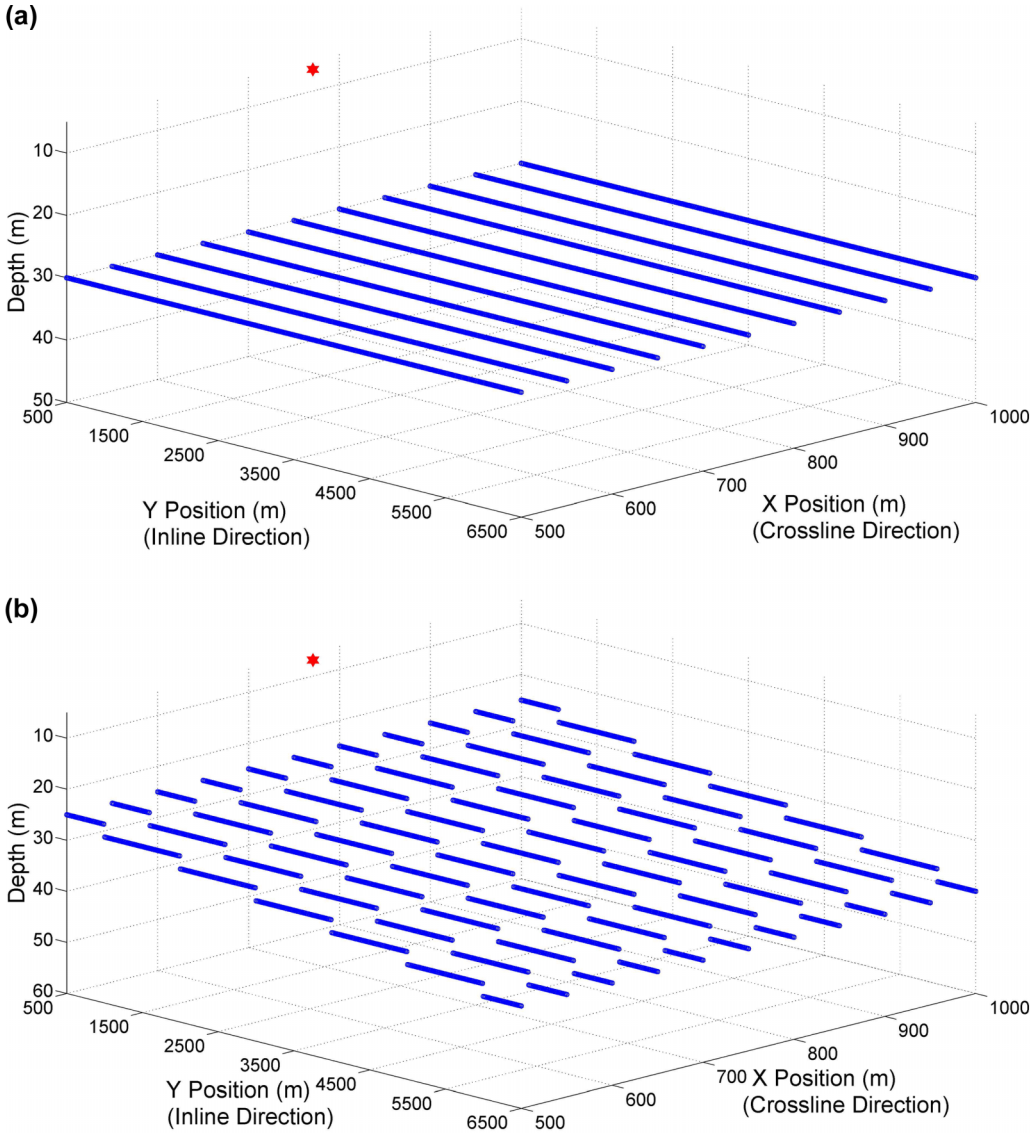

Figure 4 Data acquisition schemes for (a) the horizontal streamer case and (b) the slanted streamer case. The red star designates the source position (750 m, 750 m, 5 m). Inline (*Y*-direction) spacing is 12.5 m, and crossline (*X*-direction) spacing is 50 m. For the slanted streamer, receivers within the initial 500 m in the inline direction are at $z = 25$ m, and after that, for every 1 km, the receiver depth is further increased by 2.5 m. The deepest receiver depth is 40 m at the maximum offset. Other parameters are the same as in the horizontal streamer case.

THEORY AND ALGORITHM

In marine seismic data acquisition, towed streamers, which, in reality, can be in any shape (e.g., horizontal, slanted, or even curved), are normally placed from a few metres to several tens of metres below the water surface; hence, the streamers actually record the scattered wavefield twice, i.e., once upward and the other time downward after the wavefield is reflected by the air–water interface. Due to the interference of these two wavefields, certain frequency components are suppressed or even cancelled out, and this is the well-known receiver ghost effect. Figure 1 is a schematic of this process. Undersampled wavefield is another challenge in streamer data acquisition. Usually, the crossline interval is much larger than the inline interval (in reality, the ratio of inline to crossline interval varies between 1:4 and 1:16); hence, the acquired wavefield is generally aliased in the crossline direction, which further complicates receiver deghosting.

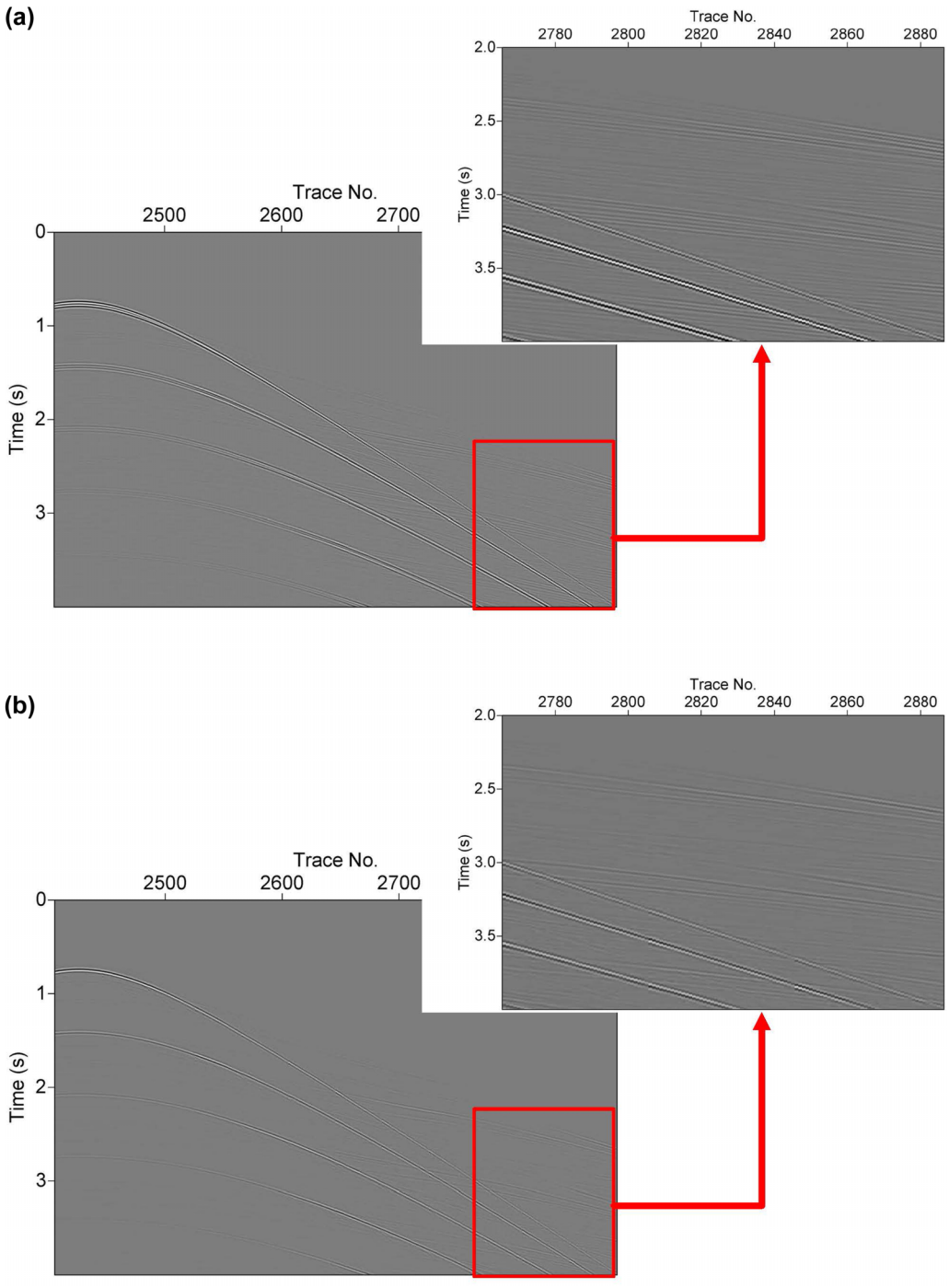

Figure 5 The central/near-offset cable in the horizontal streamer case of the modified EAGE/SEG Overthrust model (a) before and (b) after our 3D receiver deghosting.

To handle the receiver deghosting problem in a more physical manner, wave propagation phenomena should be better honoured, and this requires the undersampled wavefield challenge and the receiver ghost removal to be addressed simultaneously. Because the complete receiver ghost process happens only in water, which can be treated as an isotropic and homogeneous medium, acoustic wave propagation theory is sufficient to describe it, and we choose the Rayleigh

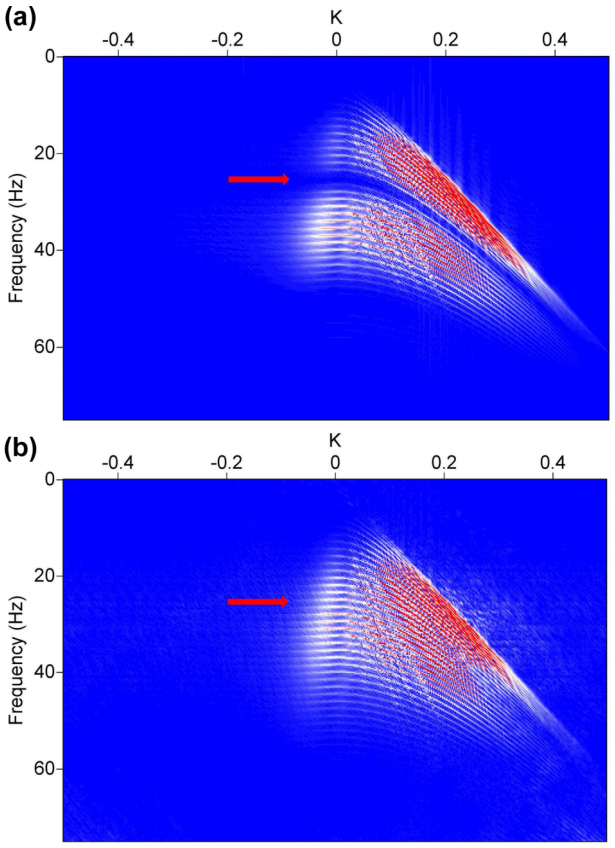

Figure 6 FK spectra of the traces from the central/near-offset cable in the synthetic horizontal streamer case from the modified EAGE/SEG Overthrust model: (a) before and (b) after 3D receiver deghosting. The red arrow points to the frequency notch area.

integral (see, e.g., the work of Gisolf and Verschuur (2010)) as our wave propagation modelling engine. For the Rayleigh integral to hold, two conditions have to be met: its integral surface has to be a plane and wavefield sampling on this planar surface has to be dense. We propose to directly solve for the densely sampled upgoing wavefield at the water surface since it can meet these two conditions simultaneously: the wavefield is dense by our definition, and the water surface, in reality, is close to a planar surface at the wavelengths under study. With this in mind, the total scattered wavefield recorded by receivers can then be described as summation of the backward propagated wavefield from the water surface to the receiver locations and the forward propagated wavefield, taking into account surface reflections, from the water surface to the receiver locations. This idea of treating the water surface as a mirror reflector was also adopted by some other researchers (see, e.g., the works of Poole (2013) and Hardwick *et al.* (2015)). Note that, in our model, streamers in any shape can be handled because the integral can be accurately evaluated for any receiver location as long as the corresponding wave propagation operator is provided. Figure 2 shows a schematic of the receiver ghost process using our model (note that direct arrivals are assumed to have been removed), and mathematically, it can be described as

$$\mathbf{b} = \mathbf{S}\mathbf{P}^{-}\mathbf{h} + \mathbf{S}\mathbf{P}^{+}\mathbf{R}\mathbf{h} = \mathbf{S}(\mathbf{P}^{-} + \mathbf{P}^{+}\mathbf{R})\mathbf{h}, \tag{1}$$

where $\mathbf{b}$ is a vector containing the measured data at known receiver depths; $\mathbf{h}$ is the dense wavefield vector at the water surface; $\mathbf{S}$ is a subsampling matrix corresponding to the real data acquisition scheme in both the inline and the crossline directions; $\mathbf{P}^{-}$ and $\mathbf{P}^{+}$ are the backward and forward one-way wave propagation matrices from the water surface to the predefined dense receiver locations, which cover the actual receiver locations; and $\mathbf{R}$ is the water surface reflectivity matrix. Although $\mathbf{h}$ is a vector in equation (1), it actually consists of a 3D shot gather $f(g_x, g_y, t)$ where g_x and g_y are the x and y positions of the receiver at the water surface.

Because of the existence of $\mathbf{S}$ in equation (1), the measured data is undersampled, i.e., $\dim(\mathbf{b}) < \dim(\mathbf{h})$; hence, matrix $\mathbf{S}(\mathbf{P}^{-} + \mathbf{P}^{+}\mathbf{R})$ is generally not mathematically invertible. To overcome this mathematical hurdle, we propose to frame the receiver deghosting problem as the following equations:

$$\min_u \left\| \mathbf{A}\mathbf{u} - \mathbf{b} \right\|_2 \qquad \text{s.t. } \|\mathbf{u}\|_1 < \tau, \tag{2}$$

with

$$\mathbf{A} = \mathbf{S}(\mathbf{P}^{-} + \mathbf{P}^{+}\mathbf{R})\mathbf{D}. \tag{3}$$

In equations (2) and (3), $\mathbf{u}$ is a vector containing the encoded dense wavefield at the water surface, and $\mathbf{D}$ is a transformation matrix, which yields $\mathbf{h} = \mathbf{D}\mathbf{u}$. The key to the success of equation (2) is to find a suitable redundant dictionary so that the encoded wavefield $\mathbf{u}$ in this dictionary is a sparse representation of the dense wavefield $\mathbf{h}$ at the water surface.

In our algorithm, we encode this dense wavefield per crossline slice, i.e., the data slice perpendicular to the streamer cables, and every crossline slice has its own representation. Together with the transformation matrix $\mathbf{D}$, this encoding step is expressed mathematically as

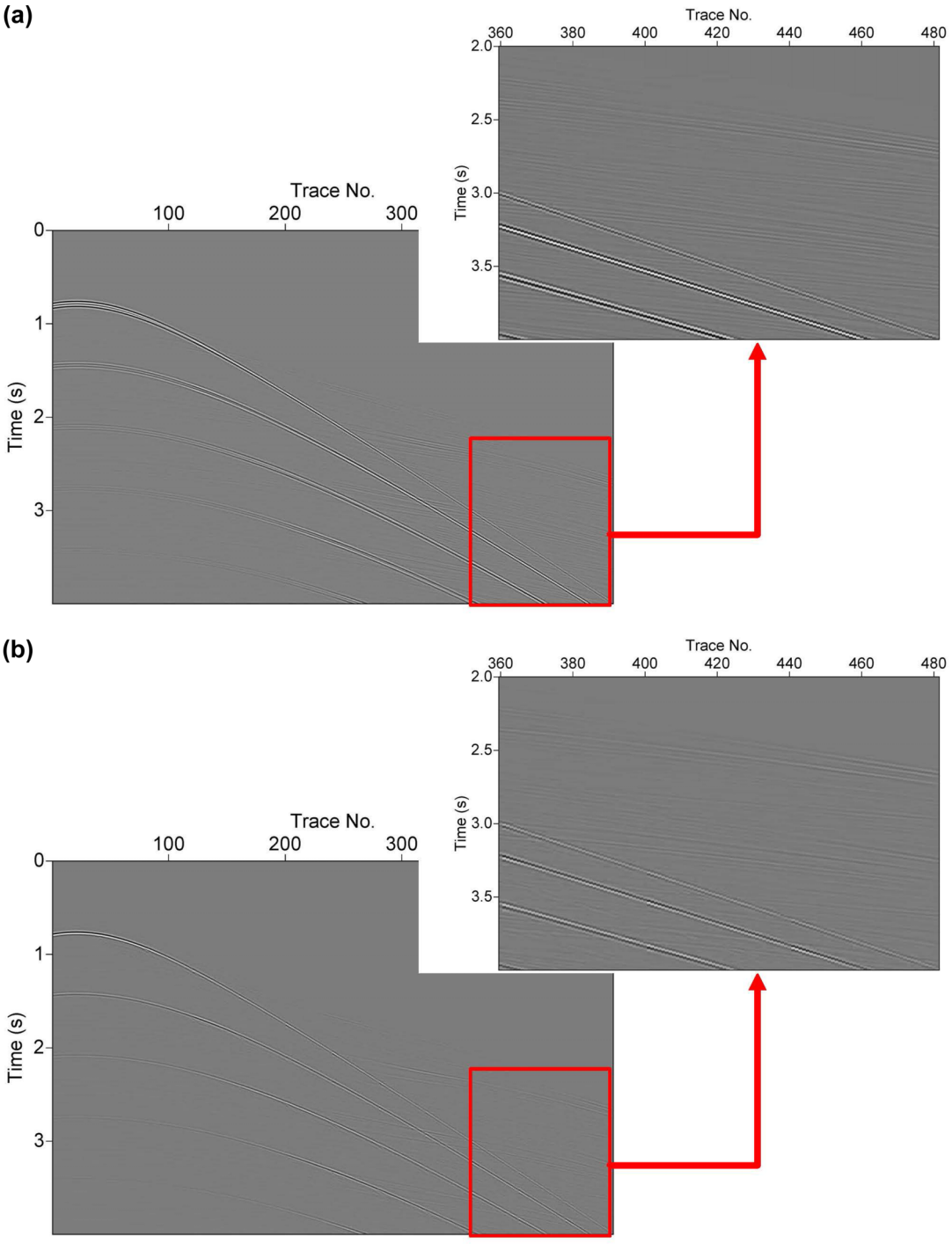

Figure 7 The first/furthest-offset cable in the horizontal streamer case of the modified EAGE/SEG Overthrust model (a) before and (b) after our 3D receiver deghosting.

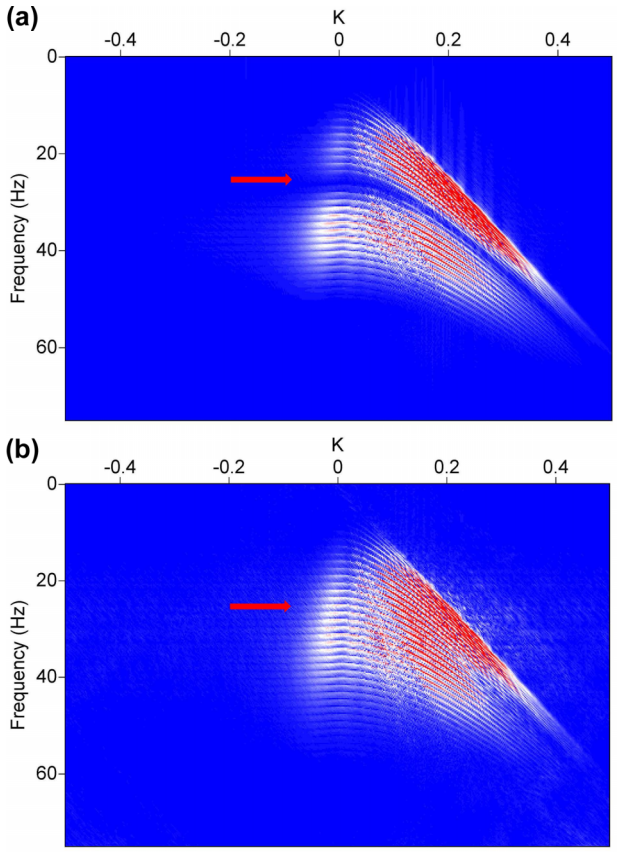

Figure 8 FK spectra of the traces from the first/furthest-offset cable in the synthetic horizontal streamer case of the modified EAGE/SEG Overthrust model: (a) before and (b) after 3D receiver deghosting. The red arrow points to the frequency notch area.

$$\mathbf{h} = \begin{bmatrix} \mathbf{h}_{slice\ 1} \\ \mathbf{h}_{slice\ 2} \\ \vdots \\ \mathbf{h}_{slice\ n-1} \\ \mathbf{h}_{slice\ n} \end{bmatrix} = \mathbf{D}\mathbf{u} = \begin{bmatrix} \mathbf{D}_{2d} & 0 & \cdots & 0 & 0 \\ 0 & \mathbf{D}_{2d} & & 0 & 0 \\ \vdots & & \ddots & & \vdots \\ 0 & 0 & & \mathbf{D}_{2d} & 0 \\ 0 & 0 & \cdots & 0 & \mathbf{D}_{2d} \end{bmatrix} \begin{bmatrix} \mathbf{u}_{slice\ 1} \\ \mathbf{u}_{slice\ 2} \\ \vdots \\ \mathbf{u}_{slice\ n-1} \\ \mathbf{u}_{slice\ n} \end{bmatrix}, \tag{4}$$

where $\mathbf{u}_{slice\ i}$ is a vector containing the wavefield representation of crossline slice i of the dense wavefield and $\mathbf{D}_{2d}$ is the corresponding matrix that transforms the encoded wavefield $\mathbf{u}_{slice\ i}$ to wavefield $\mathbf{h}_{slice\ i}$, which contains slice i of the dense wavefield at the water surface.

We propose a redundant extended Radon dictionary for our algorithm to work with. The building blocks of this new dictionary are as follows:

$$f_1(x) = \tau + px, \tag{5}$$

$$f_{g,h}(x) = \tau + q(x - a_h)^g, \quad g > 1, \tag{6}$$

where a_h is an apex location of the gth-order Radon curve. Linear Radon atom, which is described by equation (5), is always considered in our calculation, and on top of it, we have freedom to include some higher order Radon atoms with shifted apices, as described by equation (6). In other words, our intention is to decompose the data $\mathbf{h}_{slice\ i}$ into wavefronts depicted by different Radon curves. Using our redundant extended Radon dictionary, $\mathbf{D}_{2d}$ in equation (4) can be decomposed into a combination of contributions of different building blocks, which is expressed now as

$$\mathbf{D}_{2d} = \mathbf{F}^{-1}\mathbf{O}^{-1} \left[\mathbf{L}_1\ \mathbf{L}_{2,1}\ \mathbf{L}_{2,2} \cdots \mathbf{L}_{2,n_2}\ \mathbf{L}_{3,1}\ \cdots \mathbf{L}_{3,n_3}\ \cdots \mathbf{L}_{g,n_g} \right] \mathbf{O}\mathbf{F}, \tag{7}$$

where

$$\mathbf{L}_1 = \begin{bmatrix} \mathbf{L}_{1,\omega_1} & 0 & \cdots & 0 & 0 \\ 0 & \mathbf{L}_{1,\omega_2} & & 0 & 0 \\ \vdots & & \ddots & & \vdots \\ 0 & 0 & & \mathbf{L}_{1,\omega_{N_{max}-1}} & 0 \\ 0 & 0 & \cdots & 0 & \mathbf{L}_{1,\omega_{N_{max}}} \end{bmatrix}, \tag{8}$$

with

$$\mathbf{L}_{1,\omega_i} = \begin{bmatrix} e^{-i\omega_i x_1 p_1} & e^{-i\omega_i x_1 p_2} & \cdots & e^{-i\omega_i x_1 p_{M_1-1}} & e^{-i\omega_i x_1 p_{M_1}} \\ e^{-i\omega_i x_2 p_1} & e^{-i\omega_i x_2 p_2} & & e^{-i\omega_i x_2 p_{M_1-1}} & e^{-i\omega_i x_2 p_{M_1}} \\ \vdots & & \ddots & \vdots & \\ e^{-i\omega_i x_{N-1} p_1} & e^{-i\omega_i x_{N-1} p_2} & & e^{-i\omega_i x_{N-1} p_{M_1-1}} & e^{-i\omega_i x_{N-1} p_{M_1}} \\ e^{-i\omega_i x_N p_1} & e^{-i\omega_i x_N p_2} & \cdots & e^{-i\omega_i x_N p_{M_1-1}} & e^{-i\omega_i x_N p_{M_1}} \end{bmatrix}, \tag{9}$$

$$1 \le i \le N_{max},$$

and where

$$\mathbf{L}_{s,m} = \begin{bmatrix} \mathbf{L}_{s,m,\omega_1} & 0 & \cdots & 0 & 0 \\ 0 & \mathbf{L}_{s,m,\omega_2} & & 0 & 0 \\ \vdots & & \ddots & & \vdots \\ 0 & 0 & & \mathbf{L}_{s,m,\omega_{N_{max}-1}} & 0 \\ 0 & 0 & \cdots & 0 & \mathbf{L}_{s,m,\omega_{N_{max}}} \end{bmatrix}, \tag{10}$$

$$2 \le s \le g,\ 1 \le m \le n_g,$$

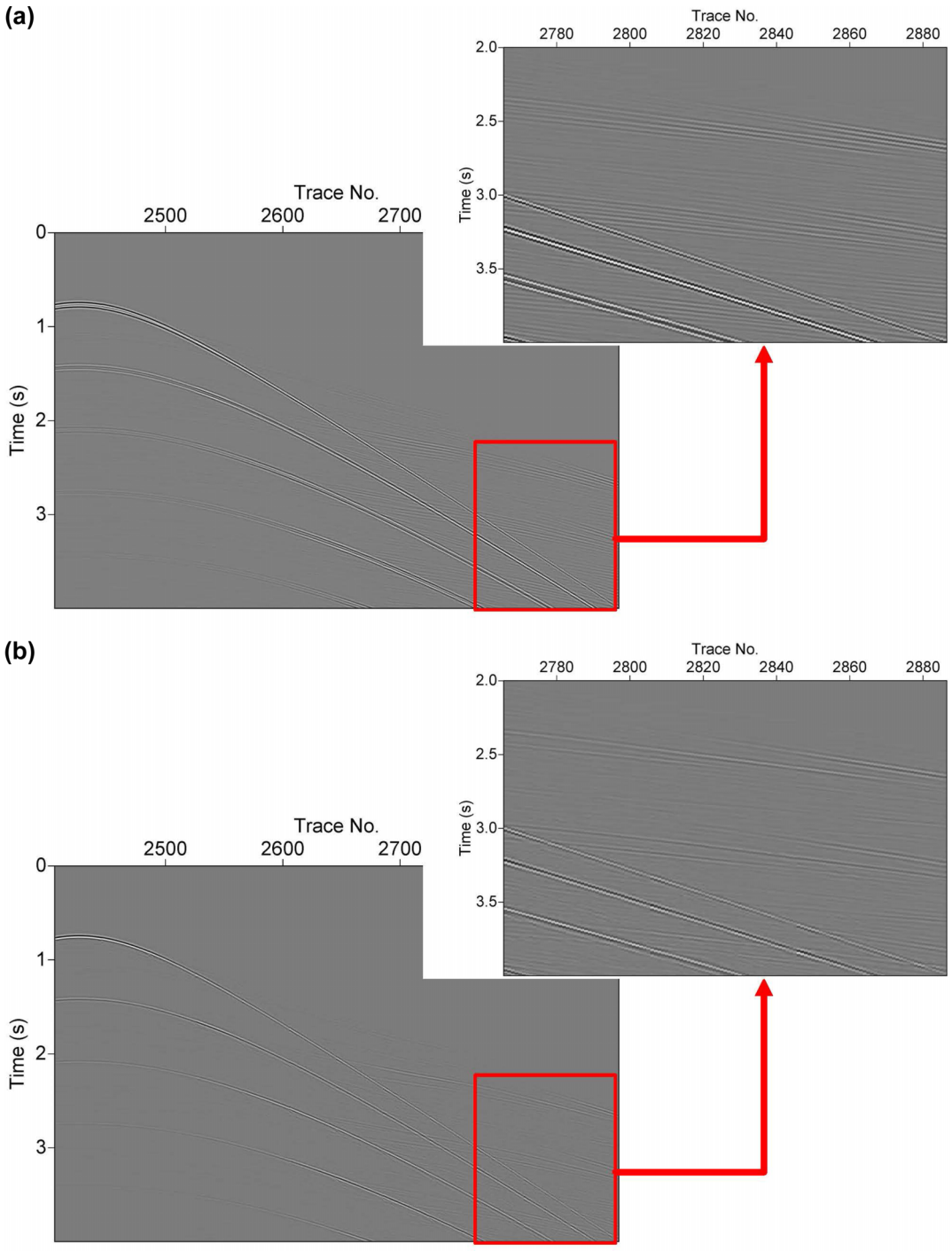

Figure 9 The central/near-offset cable in the slanted streamer case of the modified EAGE/SEG Overthrust model (a) before and (b) after our 3D receiver deghosting.

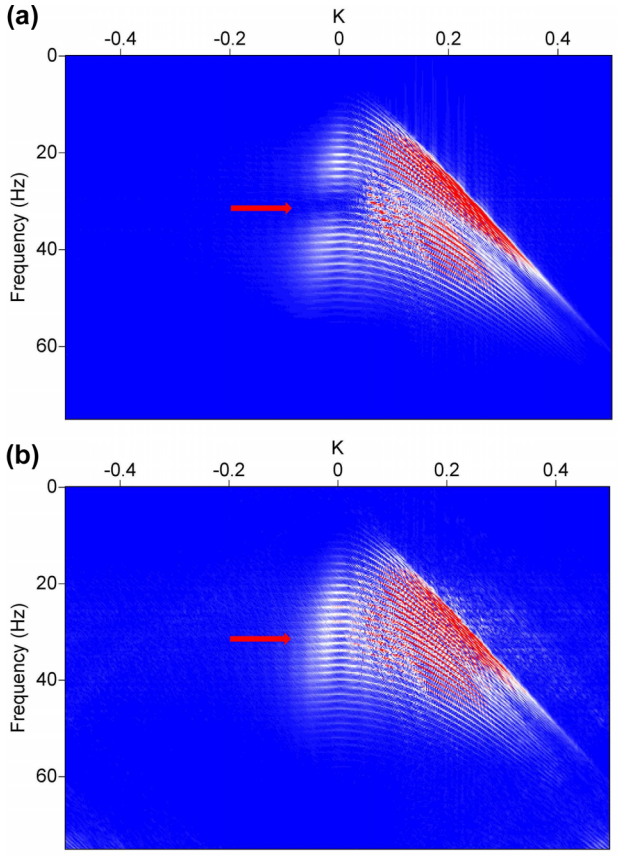

Figure 10 FK spectra of the traces from the central/near-offset cable in the synthetic slanted streamer case of the modified EAGE/SEG Overthrust model: (a) before and (b) after 3D receiver deghosting. The red arrow points to the frequency notch area.

with

$$\mathbf{L}_{s,m,\omega_i} = \begin{bmatrix} e^{-i\omega_i(x_1-a_m)^S q_1} & e^{-i\omega_i(x_1-a_m)^S q_2} & \cdots & e^{-i\omega_i(x_1-a_m)^S q_{M_s-1}} & e^{-i\omega_i(x_1-a_m)^S q_{M_s}} \\ e^{-i\omega_i(x_2-a_m)^S q_1} & e^{-i\omega_i(x_2-a_m)^S q_2} & & e^{-i\omega_i(x_2-a_m)^S q_{M_s-1}} & e^{-i\omega_i(x_2-a_m)^S q_{M_s}} \\ \vdots & & \ddots & \vdots & \\ e^{-i\omega_i(x_{N-1}-a_m)^S q_1} & e^{-i\omega_i(x_{N-1}-a_m)^S q_2} & & e^{-i\omega_i(x_{N-1}-a_m)^S q_{M_s-1}} & e^{-i\omega_i(x_{N-1}-a_m)^S q_{M_s}} \\ e^{-i\omega_i(x_N-a_m)^S q_1} & e^{-i\omega_i(x_N-a_m)^S q_2} & \cdots & e^{-i\omega_i(x_N-a_m)^S q_{M_s-1}} & e^{-i\omega_i(x_N-a_m)^S q_{M_s}} \end{bmatrix}, \quad 1 \le i \le N_{max}, \tag{11}$$

where ω_i is the angular frequency. In equation (7), **F** is the discrete Fourier transformation (DFT) matrix; $\mathbf{F}^{-1}$ is the inverse DFT matrix; $[\mathbf{L}_1 \ \mathbf{L}_{2,1} \ \mathbf{L}_{2,2} \ \cdots \ \mathbf{L}_{2,n_2} \ \mathbf{L}_{3,1} \ \cdots \ \mathbf{L}_{3,n_3} \ \cdots \ \mathbf{L}_{g,n_g}]$ is the redundant extended Radon matrix, where $\mathbf{L}_1$ is the linear Radon transformation matrix as detailed in equations (8) and (9), and $\mathbf{L}_{g,n_g}$ is the gth-order Radon transformation matrix with the curve apex at a_{n_g} as detailed in equations (10) and (11); **O** is a matrix that shuffles the vector to a suitable order, which the redundant extended Radon matrix can operate on; and $\mathbf{O}^{-1}$ is the inverse of **O**, which shuffles the vector back to the original order for the inverse Fourier transform.

Equations (2) to (11) form the backbone of our deghosting method, and once **u** is solved, the *in situ* deghosted wavefield $\mathbf{SP}^{-}\mathbf{Du}$ can then be easily calculated.

Equation (2) is the famous Lasso problem in mathematics (Tibshirani 1996), for which various solvers have been proposed. In our algorithm, the SPGL1 solver (van den Berg and Friedlander 2008) is used. There are two major advantages of using SPGL1. First, SPGL1 does not require calculating the inverse of **A** in equation (2) in any sense but only requires the Hermitian of A, which can be computed straightforwardly. Second, SPGL1 supports operator calculations; hence, although in our theory equations (2) to (11) are all in matrix format, in our implementation, all these calculations are done via operators, which not only saves memory but also makes the implementation much easier. However, we find that, in the SPGL1 method, the step involving projection onto a diagonally weighted 1-norm ball (L1 projection) is the dominant factor in computation speed. Therefore, we recommend replacing the original sorting-based L1 projection algorithm with the active set method, which is not only faster in terms of computational complexity but also very suitable for parallelisation. Details on our active set method-based L1 projection can be found in the Appendix.

To achieve satisfying results, it is crucial to properly build $\mathbf{P}^{-}$ and $\mathbf{P}^{+}$ in equation (3). In the Rayleigh theory, the integral aperture should be infinite, but in reality, this requirement is not practical. As a result, $\mathbf{P}^{-}$ and $\mathbf{P}^{+}$ have to take this limited aperture into consideration and different choices of implementation of these two propagation matrices will bring slightly different results. In this paper, we suggest to

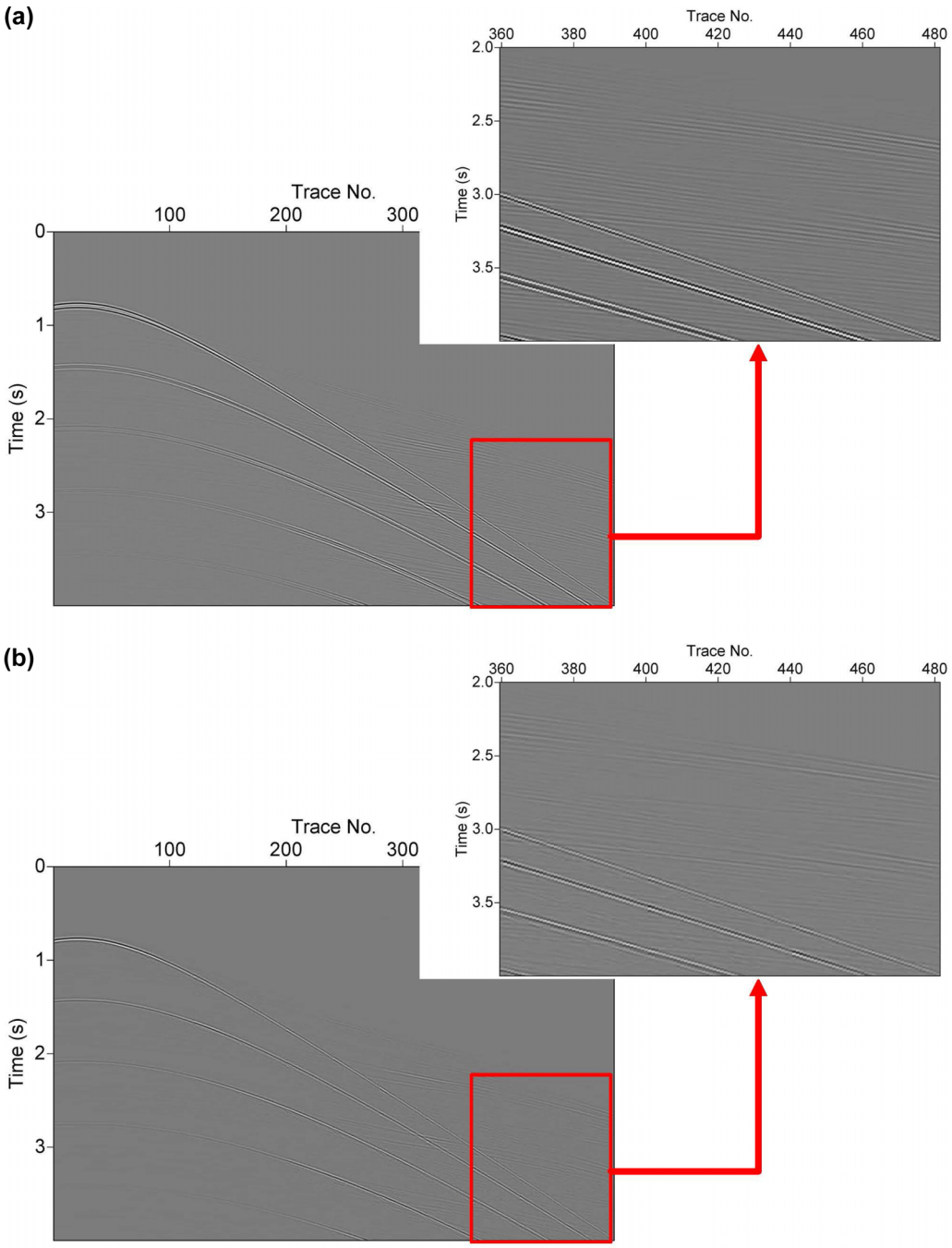

Figure 11 The first/furthest-offset cable in the slanted streamer case of the modified EAGE/SEG Overthrust model (a) before and (b) after our 3D receiver deghosting.

use weighted least-squares optimised one-way propagation operators (Thorbecke, Wapenaar and Swinnen 2004) to build $\mathbf{P}^{-}$ and $\mathbf{P}^{+}$. An advantage of using a limited aperture is that the wavefield calculation can be decoupled; for the wavefield within a certain area (even including the time direction), only a limited integral area in the integral plane needs to be considered. Therefore, in our calculations, we divide the complete solution area into overlapping small windows or volumes and then work on each one separately. In the end, all these subresults are averaged and spliced together via a trapezoidal

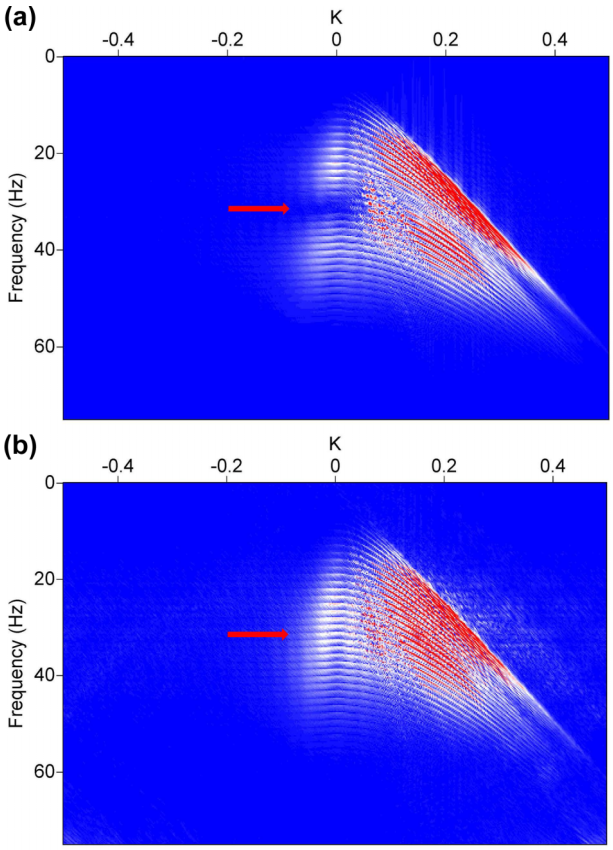

Figure 12 FK spectra of the traces from the first/furthest-offset cable in the synthetic slanted streamer case of the modified EAGE/SEG Overthrust model: (a) before and (b) after 3D receiver deghosting. The red arrow points to the frequency notch area.

weight function to form the final complete result. Two benefits can be obtained from this approach: (1) although the complete dataset may be huge, a subset can be of realistic size to be handled with limited computation resources, and (2) due to both the edge effect of the integral aperture and the limited number of building blocks in the dictionary, computation artefacts are unavoidable but can be suppressed via averaging as the sub-areas overlap.

Operator **R** in equation (3) should also be handled with care. Although in most reported methods **R** is always assumed to be $-\mathbf{I}$, in reality, its behaviour is much more complex as the water surface cannot be perfectly flat. To our knowledge, this point has not been dwelled on adequately yet (Orji, Sollner and Gelius 2013); however, we leave 3D receiver deghosting with variable **R** for future research, and for the time being, **R** is assumed to be $-\mathbf{I}$.

EXAMPLE: A MODIFIED THREE-DIMENSIONAL EAGE/SEG OVERTHRUST MODEL

We first use a realistic synthetic example from a modified 3D EAGE/SEG Overthrust model (Aminzadeh, Brac and Kunz 1997) to demonstrate our method. First of all, a 500 m-thick water layer is put on top of the original 3D model, and a subset of this new model is selected. The subset comprises, in the *X*-direction, between 10 km and 11.5 km (as the crossline direction in our modelling, $x \in [0\text{ m},\ 1500\text{ m}]$), and in the *Y*-direction, it comprises between 7.5 km and 14.5 km (as the inline direction, $y \in [0\text{ m},\ 7000\text{ m}]$) (Fig. 3). The corresponding density model is also built based upon this modified velocity model, with densities derived from the velocities via Gardner's equation (Gardner, Gardner and Gregory 1974), except for the water layer where the density value is set to 1000 kg/m^3. Acoustic 3D finite-difference time-domain (FDTD) modelling is used as our forward modelling engine.

Two different data acquisition schemes are considered here, i.e., using horizontal streamers and using slanted streamers. In both cases, the source wavelet is a Ricker with a 20-Hz dominant frequency, which is located at $x = 750$ m, $y = 750$ m, and $z = 5$ m. The maximum frequency used in our inversion is limited to 75 Hz. The seismic streamers cover an area of ± 250 m in the crossline direction by 6 km in the inline direction with offsets from 500 to 6500 m. The inline receiver interval is 12.5 m, and the crossline interval is 50 m. For the horizontal streamer case, the streamer depth is set at 30 m (Fig. 4a). For the slanted streamer case, due to the fact that FDTD is our simulation method, continuously varying depths cannot be easily defined. As a compromise solution, we use a quasi-slanted data acquisition scheme where receivers are all at the same depth in the crossline direction, whereas in the inline direction, the receiver depths form a staircase, i.e., within the first 500 m offset, the receivers are at 25 m depth, and after that, for every 1 km increase in offset, the receiver depths are increased by 2.5 m until they reach 40 m at maximum offset. Figure 4b shows this quasi-slanted streamer configuration in detail.

To suppress computation artefacts in our calculation, overlapping windows or sub-volumes are used. Each sub-volume comprises the entire trace and crossline aperture, whereas in the inline direction, the window length is 500 m. The first sub-volume starts at $y = 500$ m in the inline direction, and sub-volumes overlap by 300 m, moving up by 200 m in each successive window in the inline direction.

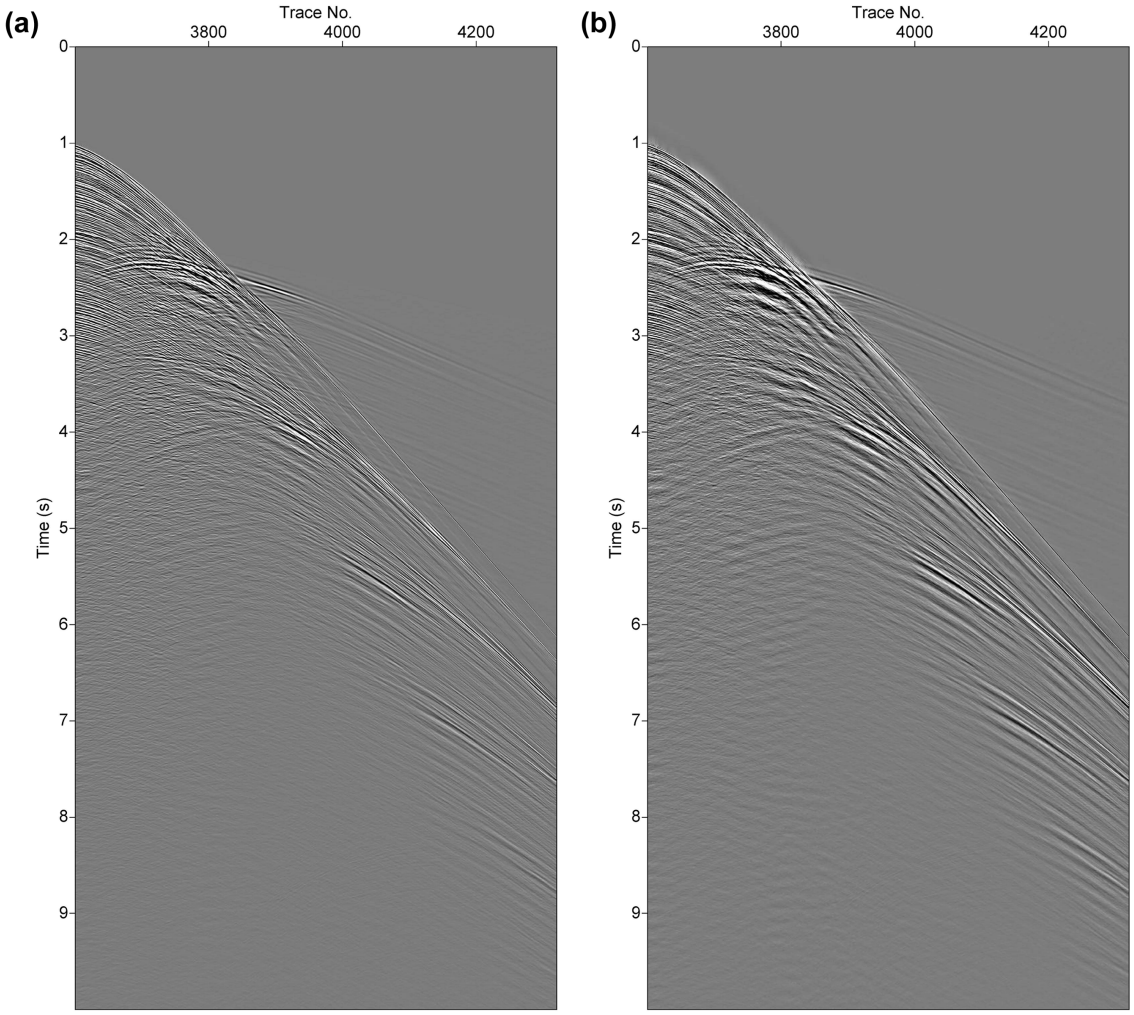

Figure 13 The central/near-offset cable of the Red Sea field data (a) before and (b) after 3D receiver deghosting.

The final deghosted result is the arithmetic average of all these sub-volumes. A 250 m by 250 m Rayleigh integral aperture is used to build propagation operators. In equation (7), the linear Radon term plus three parabolic Radon terms are used. Apex values in the parabolic Radon terms can be selected in many ways, and in this example, they are determined using the idea of matching pursuit (Mallat and Zhang 1993). For each spatial window, the central crossline slice in the inline direction is picked out first (for instance, if there are three crossline slices in this spatial window, $y = y_1$, $y = y_1+\Delta y$, $y = y_1+2\Delta y$, then pick out the crossline slice $y = y_1+\Delta y$). Next, we calculate the parabolic Radon contribution with the apex scanned through the whole crossline range and then pick out the apex value that leads to the smallest residual on this crossline slice. Contributions from this apex value are deducted from the current crossline slice, and the residual slice is used as the new crossline slice. This process is repeated until all needed apex values have been selected.

Figures 5–12 show the results for both the horizontal streamer and the quasi-slanted streamer case. Figure 5 shows the central/near-offset cable in the horizontal streamer situation before and after our 3D receiver deghosting. Figure 6 shows the FK spectra in Fig. 5, and there, it is clearly shown that the receiver ghost notch has been nicely recovered. Figure 7 shows the first cable, i.e., the furthest-offset cable, in the horizontal streamer situation before and after our 3D receiver deghosting, and Fig. 8 shows its corresponding FK spectra, from which nice receiver ghost notch recovery can also be found easily. Figures 9–12 show the results in the slanted streamer situation in the same manner as in Figs. 5–8.

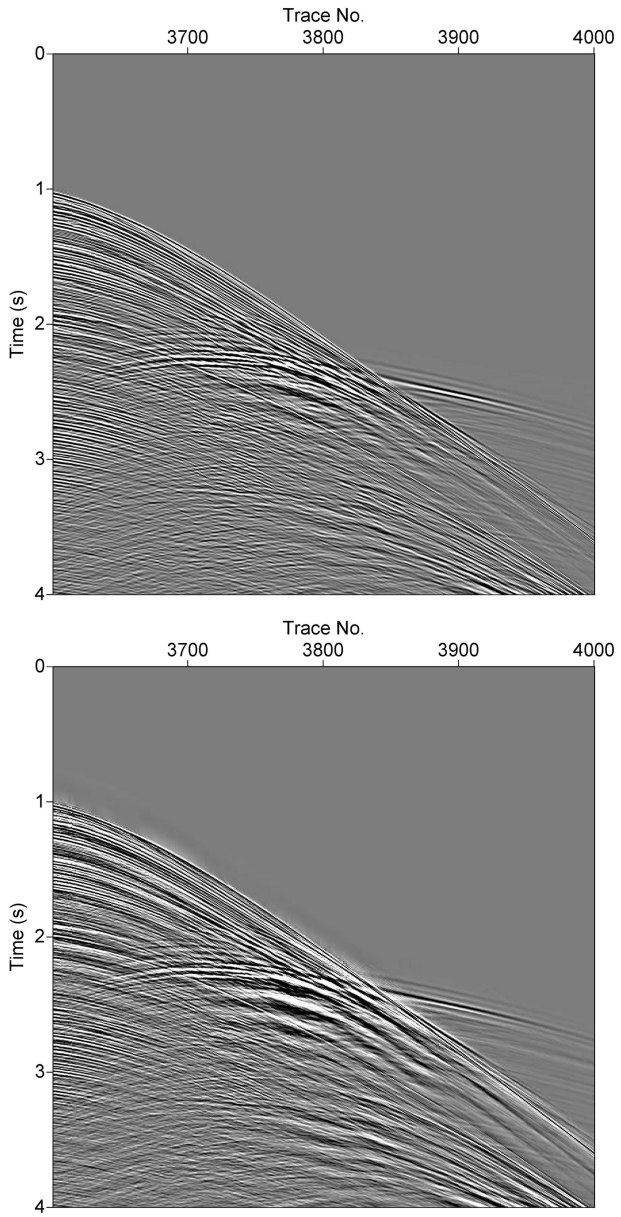

Figure 14 Zoom-in view of the first 4 s window of the initial 400 traces of the central/near-offset cable shown in Fig. 13.

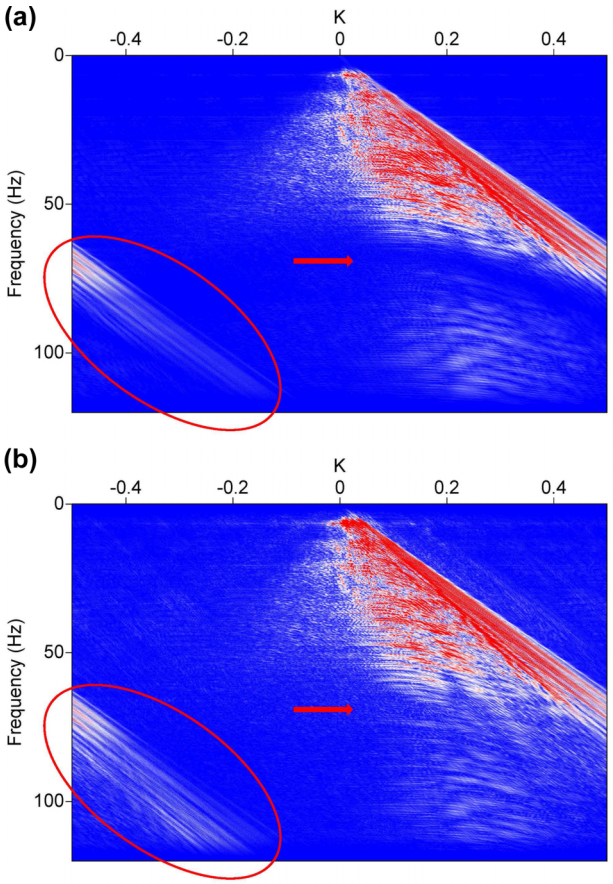

Figure 15 FK spectra from the central/near-offset cable in the Red Sea field data (a) before and (b) after 3D receiver deghosting. The red arrow points to the frequency notch, and the red ellipse highlights the area where the inline aliased data also show spectral broadening.

EXAMPLE: A RED SEA FIELD DATA TEST

For the field data case, a 3D shot gather from the Red Sea is used to demonstrate our deghosting method. The data comprise ten streamers with a nominal group spacing of 12.5 m, a streamer spacing of 100 m, and a streamer length of 9 km. This shot gather has 7200 traces in total. The air gun source depth is 9 m with the streamers at a nominal depth of 12 m. The time sampling rate is 2 ms with a trace length of 10 s. In our 3D receiver deghosting procedure, the wavefield at the water surface is parameterised on a 6.25 m by 6.25 m grid, and the maximum frequency used in our inversion is 120 Hz. As in the synthetic data example, a square 250 m by 250 m wave propagation aperture is used, and the water velocity is set to 1500 m/s. We still assume **R** to be $-\mathbf{I}$. The bubble signals were not removed prior to our 3D receiver deghosting as bubble signals also fit into our receiver ghost model and hence can also be properly receiver deghosted. As for the synthetic example above, the linear Radon term plus three parabolic terms are used as the building blocks in our dictionary, and the apex value selection is also done in a similar fashion. The data sub-volumes used in this example comprise the entire crossline range, with a 500 m window in the inline direction and a 5 s time window. The sub-volume step in the inline direction is 100 m, and in the time

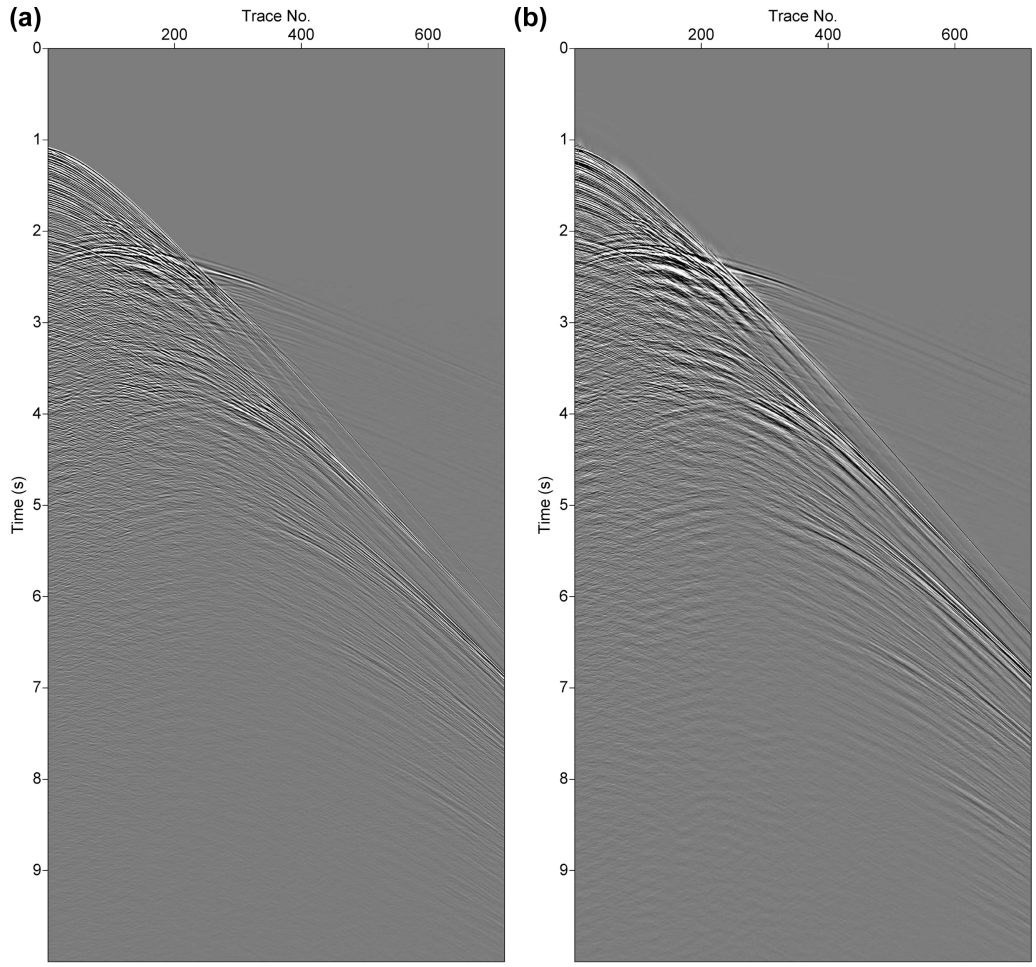

Figure 16 The first/furthest-offset cable in the Red Sea field data (a) before and (b) after 3D receiver deghosting.

direction, it is 2.5 s, i.e., sub-volumes overlap by 400 m in the inline direction and by 2.5 s in time.

Figure 13 shows data from the central/near-offset cable before and after 3D receiver deghosting, and Fig. 14 shows the zoom-in view of the first 4 s time window of the initial 400 traces in Fig. 13. Figure 15 shows the FK spectra in Fig. 13. Figures 16–18 show results of the first/furthest-offset cable in the same manner as in Figs. 13–15. In Figs. 15 and 18, the receiver deghosting effect is clearly visible as the notch has been well recovered and the overall spectrum has been broadened. Note that the inline aliased part of the data, visible in the bottom left corner in the FK domain (Figs. 15 and 18), has also been properly handled and shows the appropriate spectral whitening following deghosting.

CONCLUSIONS

In this paper, we have proposed a novel 3D receiver deghosting algorithm that is capable of dealing with both horizontal and slanted streamers in a theoretically consistent manner. Our algorithm fully honours wave propagation phenomena during marine streamer acquisition in a true 3D sense, and it implicitly and self-consistently reconstructs the deghosted wavefield at the water surface. Mathematically, our method frames the receiver deghosting problem as a Lasso problem, and the SPGL1 method is used as its mathematical solver. We also proposed a new redundant dictionary, i.e., the redundant extended Radon dictionary, as our basis dictionary. We have successfully demonstrated our method on a modified 3D EAGE/SEG Overthrust model and a Red Sea field dataset.

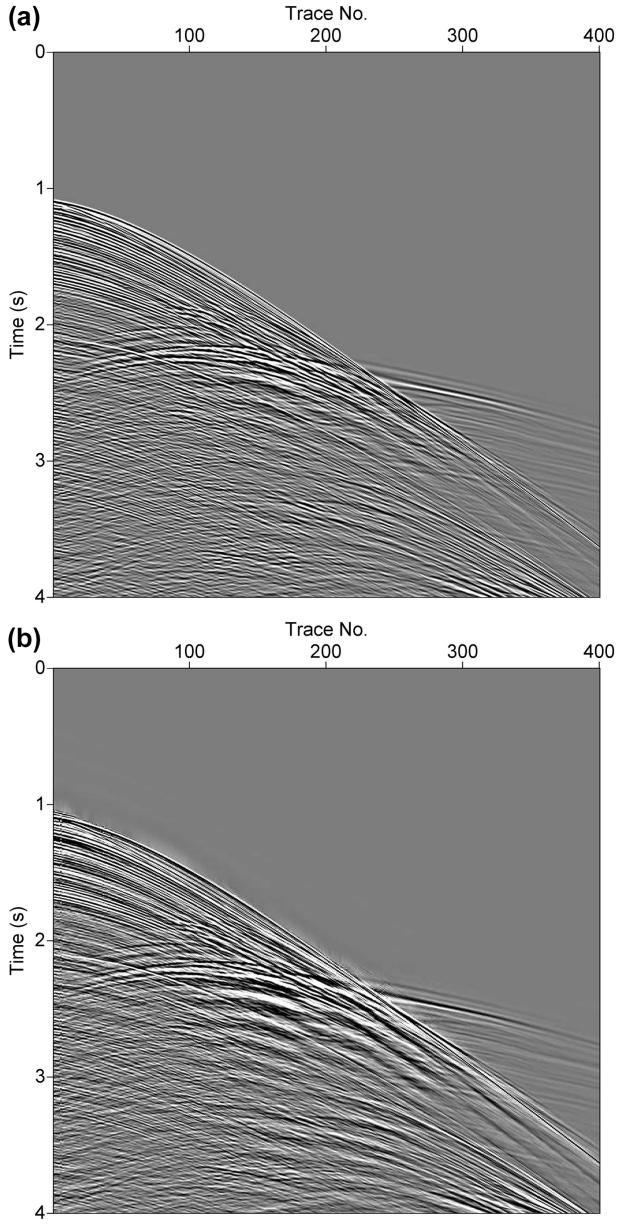

Figure 17 Zoom-in view of the first 4 s window of the initial 400 traces of the first/furthest-offset cable shown in Fig. 16.

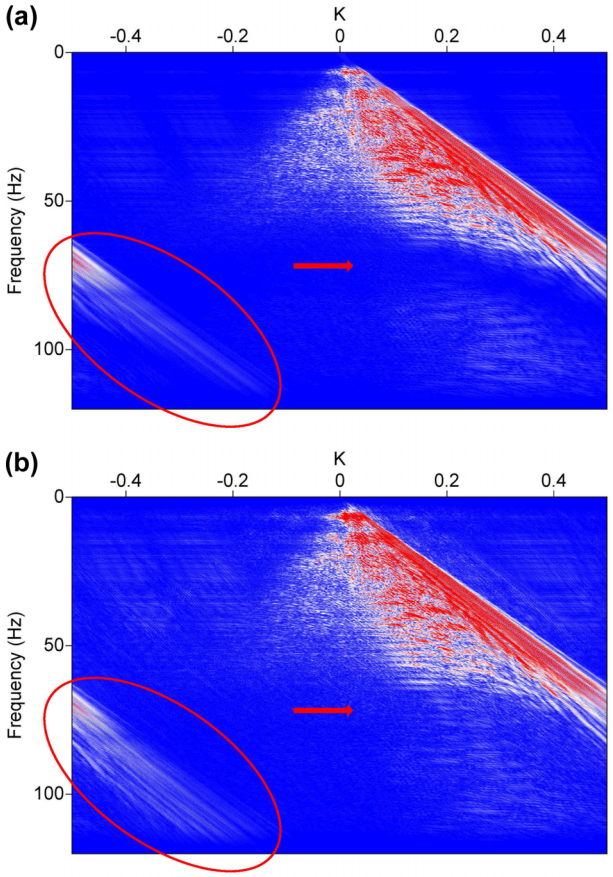

Figure 18 FK spectra from the first/furthest-offset cable in the Red Sea field data (a) before and (b) after 3D receiver deghosting. The red arrow points to the frequency notch, and the red ellipse highlights the area where the inline aliased data also show spectral broadening.

ACKNOWLEDGEMENTS

The authors would like to thank Roald van Borselen and Mike Jervis for reviewing their paper, Bryan Maddison for providing the Red Sea field data, and Saudi Aramco for permission to publish this work. A patent has been published (Publication No. US-2017-0276818-A1).

ORCID

Yimin Sun http://orcid.org/0000-0002-6663-6146

REFERENCES

Aminzadeh F., Brac J. and Kunz T. 1997. *3D Salt and Overthrust Models. SEG/EAGE Modelling Series, No. 1: Distribution CD of Salt and Overthrust Models, SEG Book Series*. Tulsa, OK: Society of Exploration Geophysicists.

Amundsen L., Rosten T., Robertsson J.O.A. and Kragh E. 2005. Rough-sea deghosting of streamer seismic data using pressure gradient approximations. *Geophysics* **70**, V1–V9.

Amundsen L. and Zhou H. 2013. Low-frequency seismic deghosting. *Geophysics* **78**, WA15–WA20.

Amundsen L., Weglein A.B. and Reitan A. 2013a. On seismic deghosting using integral representation for the wave equation: use of Green's functions with Neumann or Dirichlet boundary conditions. *Geophysics* **78**, T89–T98.

Amundsen L., Zhou H., Reitan A. and Weglein A.B. 2013b. On seismic deghosting by spatial deconvolution. *Geophysics* **78**, V267–V271.

Beasley C. and Coates R. 2014. Wave equation receiver deghosting—Application to field data. Second EAGE/SBGf Workshop 2014, Expanded Abstracts, We G04.

Beasley C., Coates R. and Ji Y. 2013a. Wave equation receiver deghosting. 75th EAGE annual international meeting, Expanded Abstracts, Th 08 12.

Beasley C.J., Coates R., Ji Y. and Perdomo J. 2013b. Wave equation receiver deghosting: a provocative example. 83rd SEG annual international meeting, Expanded Abstracts, 4226–4230.

van den Berg E. and Friedlander M.P. 2008. Probing the Pareto frontier for basis pursuit solutions. *SIAM Journal on Scientific Computing* **31**, 890–912.

van den Berg E. and Friedlander M.P. 2011. Sparse optimization with least-squares constraints. *SIAM Journal on Optimization* **21**, 1201–1229.

Berkhout A.J. and Blacquiere G. 2014. Combining deblending with multi-level source deghosting. 84th SEG annual international meeting, Expanded Abstracts, 41–45.

Carlson D.H., Long A., Sollner W., Tabti H., Tenghamn R. and Lunde N. 2007. Increased resolution and penetration from a towed dual-sensor streamer. *First Break* **25**, 71–77.

Condat L. 2016. Fast projection onto the simplex and the L1 ball. *Mathematical Programming Series A* **158**, 575–585.

Egan M., El-Kasseh K.G. and Moldoveanu N. 2007. Full deghosting of OBC data with over/under source acquisition. 77th SEG annual international meeting, Expanded Abstracts, 31–35.

Ferber R., Caprioli P. and West L. 2013. L1 pseudo-Vz estimation and deghosting of single-component marine towed-streamer data. *Geophysics* **78**, WA21–WA26.

Fokkema J.T. and van den Berg P.M. 1993. *Seismic Applications of Acoustic Reciprocity*. Elsevier.

Gardner G.H.F., Gardner L.W. and Gregory A.R. 1974. Formation velocity and density — the diagnostic basics for stratigraphic traps. *Geophysics* **39**, 770–780.

Gisolf A. and Verschuur D.J. 2010. *The Principles of Quantitative Acoustic Imaging*. EAGE Publications BV.

Hardwick A., Chavron P., Masoomzadeh H., Aiyepeku A., Cox P. and Laha S. 2015. Accounting for sea surface variation in deghosting—A novel approach applied to a 3D dataset offshore west Africa. 85th SEG annual international meeting, Expanded Abstracts, 4615–4619.

Kamil Y.I. and Caprioli P. 2014. Optimal deghosting robust to nonstationary noise from multimeasurement streamer data. 84th SEG annual international meeting, Expanded Abstracts, 4228–4232.

Kamil Y.I., Yadari N.E. and Vassallo M. 2014. Bayesian deghosting approach for multimeasurement streamer data. 84th SEG annual international meeting, 4233–4237.

Kragh E., Robertsson J., Laws R., Amundsen L., Rosten T., Davies T. et al. 2004. Rough-sea deghosting using wave heights derived from low-frequency pressure recordings—A case study. 74th SEG annual international meeting, Expanded Abstracts, 1309–1312.

Mallat S.G. and Zhang Z. 1993. Matching pursuits with time-frequency dictionaries. *IEEE Transactions on Signal Processing* **41**, 3397–3415.

Michelot C. 1986. A finite algorithm for finding the projection of a point onto the canonical simplex of R^n. *Journal of Optimization Theory and Applications* **50**, 195–200.

Orji O.C., Sollner W. and Gelius L.J. 2013. Sea surface reflection coefficient estimation. 83rd SEG annual international meeting, Expanded Abstracts, 51–55.

Ozbek A., Vassallo M., Ozdemir K., van Manen D.J. and Eggenberger K. 2010. Crossline wavefield reconstruction from multi-component streamer data: joint interpolation and 3d up/down separation by generalized matching pursuit. 80th SEG annual international meeting, Expanded Abstracts, 3599–3603.

Poole G. 2013. Pre-migration receiver de-ghosting and re-datuming for variable depth streamer data. 83rd SEG annual international meeting, Expanded Abstracts, 4216–4220.

Poole G. 2014. Wavefield separation using hydrophone and particle velocity components with arbitrary orientation. 84th SEG annual international meeting, Expanded Abstracts, 1858–1862.

Posthumus B.J. 1993. Deghosting using a twin streamer configuration. *Geophysical Prospecting* **41**, 267–286.

Ramirez A.C. and Weglein A.B. 2009. Green's theorem as a comprehensive framework for data reconstruction, regularization, wavefield separation, seismic interferometry, and wavelet estimation: a tutorial. *Geophysics* **74**, W35–W62.

Rickett J. 2014. Successes and challenges in 3D interpolation and deghosting of single component marine-streamer data. 84th SEG annual international meeting, Expanded Abstracts, 3599–3604.

Riyanti C.D., van Borselen R.G., van den Berg P.M. and Fokkema J.T. 2008. Pressure wavefield deghosting for non-horizontal streamers. 78th SEG annual international meeting, Expanded Abstracts, 2652–2656.

Roberts G.A. and Goulty N.R. 1990. Directional deconvolution of marine seismic reflection data: North Sea example. *Geophysical Prospecting* **38**, 881–888.

Robertsson J.O.A., Moore I., Vassallo M., Özdemir K., van Manen D.J. and Özbek A. 2008. On the use of multicomponent streamer recordings for reconstruction of pressure wavefields in the crossline direction. *Geophysics* **73**, A45–A49.

Soubaras R. 1996. Ocean bottom hydrophone and geophone processing. 66th SEG annual international meeting, Expanded Abstracts, 24–27.

Soubaras R. 2010. Deghosting by joint deconvolution of a migration and a mirror migration. 80th SEG annual international meeting, Expanded Abstracts, 3406–3410.

Tibshirani R. 1996. Regression shrinkage and selection via the lasso. *Journal of the Royal Statistical Society Series B* **58**, 267–288.

Thorbecke J.W., Wapenaar K. and Swinnen G. 2004. Design of one-way wavefield extrapolation operators, using smooth functions in WLSQ optimization. *Geophysics* **69**, 1037–1045.

Wang P. and Peng C. 2012. Premigration deghosting for marine towed streamer data using a bootstrap approach. 82nd SEG annual international meeting, Expanded Abstracts, 1–5.

Wang P., Ray S. and Nimsaila K. 2014. 3D joint deghosting and crossline interpolation for marine single-component streamer data. 84th SEG annual international meeting, Expanded Abstracts, 3594–3598.

Weglein A.B., Shaw S.A., Matson K.H., Sheiman J.L., Stolt R.H., Tan T.H. et al. 2002. New approaches to deghosting towed streamer and ocean bottom pressure measurements. 72nd SEG annual international meeting, Expanded Abstracts, 2114–2117.

Wu Q., Lee C.C., Zhao W., Wang P. and Li Y. 2014. 3D deghosting for full-azimuth and ultra-long offset marine data. 84th SEG annual international meeting, Expanded Abstracts, 4238–4242.

APPENDIX: ACTIVE SET METHOD OF PROJECTION ONTO A DIAGONALLY WEIGHTED 1-NORM BALL

Theorem 5.3 in the work of van den Berg and Friedlander (2011) is re-stated here.

Theorem 5.3. *For fixed* $\bar{\mathbf{x}}$, λ, *and diagonal* $\mathbf{W}$,

$$\mathbf{x}(\lambda) := \operatorname{argmin}_x \frac{1}{2}\|\bar{\mathbf{x}} - \mathbf{x}\|_2^2 + \lambda\|\mathbf{W}\mathbf{x}\|_1$$
$$= \operatorname{sgn}(\bar{\mathbf{x}}) \max\left\{0,\ |\bar{\mathbf{x}}| - \lambda\,|w|\right\}.$$

The active set method of projection onto a 1-norm ball has been reported multiple times (Michelot 1986; Condat 2016), but we have not seen any report on the active set method of projection onto a diagonally weighted 1-norm ball, although this is just a generalisation of the non-weighted version. Hereby, we list the algorithm as follows:

1. Set $ABS\ X := |X|$, $ABS\ W := |W|$
2. Set active set $V := ABS\ X$, and $\rho := \frac{\sum_n \operatorname{abs} w_n \operatorname{abs} x_n - \lambda}{\sum_n \operatorname{abs} w_n \operatorname{abs} w_n}$
3. Do, while active set V changes
   - 3.1 Replace V with its subsequence ($\operatorname{abs} x_n \in V | \operatorname{abs} x_n > \rho \operatorname{abs} w_n$)
   - 3.2 Set $\rho := \frac{\sum_{\operatorname{abs} x_n \in V} \operatorname{abs} w_n \operatorname{abs} x_n - \lambda}{\sum_{\operatorname{abs} x_n \in V} \operatorname{abs} w_n \operatorname{abs} w_n}$
4. Set $x_n := \operatorname{sgn}(x_n) \max\{0, \operatorname{abs} x_n - \rho \operatorname{abs} w_n\}$